Astronomy & Astrophysics manuscript no. aa17677
February 29, 2012

Probing the anomalous extinction of four young star clusters: the use of colour-excess, main sequence fitting and fractal analysis.

B. Fernandes[1], J. Gregorio-Hetem[1], and A. Hetem Jr.[2]

[1] Universidade de São Paulo, IAG, Rua do Matão 1226, 05508-900 São Paulo, Brasil
e-mail: bfernandes@astro.iag.usp.br
[2] Universidade Federal do ABC, CECS, Rua Santa Adélia, 166, 09210-170 Santo André, SP, Brazil

Preprint online version: February 29, 2012

ABSTRACT

Aims. Four young star clusters were studied in order to characterize their anomalous extinction or variable reddening that could be due to a possible contamination by dense clouds or circumstellar effects.
Methods. The extinction law (R_V) was evaluated by adopting two methods: (i) the use of theoretical expressions based on the colour-excess of stars with known spectral type, and (ii) the analysis of two-colour diagrams, where the slope of observed colours distribution is compared to the normal distribution. An algorithm to reproduce the zero age main sequence (ZAMS) reddened colours was developed in order to derive the average visual extinction (A_V) that provides the best fitting of the observational data. The structure of the clouds was evaluated by means of statistical fractal analysis, aiming to compare their geometric structure with the spatial distribution of the cluster members.
Results. The cluster NGC 6530 is the only object of our sample showing anomalous extinction. In average, the other clusters are suffering normal extinction, but several of their members, mainly in NGC 2264, seem to have high R_V, probably due to circumstellar effects. The ZAMS fitting provides A_V values that are in good agreement with those found in the literature. The fractal analysis shows that NGC 6530 has a centrally concentrated distribution of stars that is different of the sub-structures found in the density distribution of the cloud projected in the A_V map, suggesting that the original cloud has been changed with the cluster formation. On the other hand, the fractal dimension and the statistical parameters of Berkeley 86, NGC 2244, and NGC 2264 indicate a good cloud-cluster correlation, when compared to other works based on artificial distribution of points.

Key words. open clusters: individual (NGC 2264, NGC 2244, Berkeley 86 and NGC 6530) - ISM: dust, extinction - Stars: pre-main sequence

1. Introduction

Extinction is one of the best known consequences of the dust present in the Interstellar Medium (ISM). The study of extinction on star-forming regions reveals properties of the interstellar material that leads to a better understanding of the formation and evolution of stars.

Each line-of-sight has an extinction law, which is characterized by the ratio of the total-to-selective extinction $R_V = A_V$ / E(B-V) and depends on the composition of the ISM. According to Savage & Mathis (1979) its average value in the diffuse ISM is 3.1, while in denser regions it might reach values in the range $4 < R_V < 6$. Anomalous high extinction laws have been found in several star-forming regions (Neckel & Chini 1981; Chini & Krugel 1983; Chini & Wargau 1990; Pandey et al. 2000; Samal et al. 2007). Besides the differences of the ISM characteristics, high values of R_V are commonly explained by selective evaporation of small grains caused by the radiation from hot stars, or by grain growth in circumstellar environments (e.g. van den Ancker et al. 1997). The circumstellar hypothesis seems to be supported by the correlation between reddening and extinction found by Sung et al. (2000) for a sample of 30 stars. Most of these objects had their SED well fitted by assuming $R_V = 3.1$, with some exceptions that show anomalous R_V and have high extinction probably due to the circumstellar material. From the results of a polarimetric survey in the direction of the Lagoon Nebula (M8), McCall et al. (1990) estimated $R_V = 4.64 \pm 0.27$ that is attributed to circumstellar effects. This anomalous high R_V was obtained after removing the normal foreground extinction.

The dependence of the extinction law as a function of wavelength has also been widely discussed in the literature, given the interest in identifying the characteristics of different types of grains causing the extinction, as well as the need to properly correct the reddening that affects the observational data. In general a "universal extinction law", usually a power law for wavelengths larger than 1μm, has been adopted. The power law ($A_\lambda \propto \lambda^{-\beta}$) fits most extinction curves. However, it is recognized that the index β varies significantly depending on the line-of-sight. Based on data from the *Hubble Space Telescope*, Fitzpatrick & Massa (2009) investigated the extinction dependence on near-infrared (near-IR) wavelengths. They found that a "universal" law does not apply in this case and the index β has a tendency to decrease with increasing R_V. Instead of extrapolating the usual power law, Fitzpatrick & Massa (2009) suggest a different form, independent of wavelength,

that better describes the near-IR extinction (see discussion in Sect. 3.1).

One of the most important issues directly affected by the correct determination of extinction is the accuracy on distance estimation. The cluster NGC 3603, for instance, has distances found in the literature varying from 6.3 to 10.1 kpc, a discrepancy mostly due to errors on the reddening correction. Adopting the normal R_V, Melena et al. (2008) estimated a distance of 9.1 kpc for NGC 3603, while a distance of 7.6 kpc is found if they assume the anomalous extinction law $R_V = 4.3$, as proposed by Pandey et al. (2000). The correct determination of distance is crucial in the estimation of physical parameters of open clusters, like stellar masses and ages. Particularly in star-forming regions special attention must be paid to the probable occurrence of anomalous or differential extinction.

Several methods can be employed to estimate the interstellar extinction in the direction of young star clusters, which can be due to different effects: (i) the foreground in a given line-of-sight that is pervaded by interstellar material in between the cluster and the observer; (ii) the presence of a dark cloud associated to the cluster, (iii) the individual extinction caused by circumstellar material.

The use of U-B × B-V colour-colour diagram is the classical method for estimating the average extinction towards open clusters (e.g. Prisinzano et al. 2011) and it is specially useful on the lack of spectroscopic observations (e.g. Jose et al. 2011).

In addition to colour-colour diagrams in the UBV bands, two-colour diagrams (TCDs) are also interesting for the study of extinction as proposed by Chini & Wargaw (1990). These diagrams are presented in the form V-λ × B-V, where λ refers to different bands. The distribution of the stars in TCDs is roughly linear. Anomalies in the extinction law are determined from the comparison between the distribution of field stars (which follows a normal extinction law) with the distribution of the cluster members (which may follow an anomalous extinction law).

Jose et al. (2008) adopted TCDs to verify the extinction law in the direction of the cluster Stock 8, for instance. They found the same slope for the inner region of the cluster (r < 6') as well as for a larger area (r < 12') that also includes field stars. Another example is the cluster NGC 3603 for which Pandey et al. (2000) estimated $R_V = 4.3$, indicating a remarkable difference between the distribution of field stars and members of the cluster on the TCDs.

The aim of the present work is to characterize the extinction in the direction of different young star clusters, by determining the extinction law and searching for possible spatial variations. We selected four well-known clusters, whose characteristics are compiled in the *Handbook of Star forming regions* edited by Bo Reipurth (2008): Berkeley 86 is found in the Cygnus OB1 region (Reipurth & Schneider 2008); NGC 2244 is associated to the Rosette Nebula (Róman-Zúñiga & Lada 2008); NGC 2264 is related to the Mon OB1 association (Dahm 2008); and NGC 6530 is located near to the Lagoon Nebula (Tothill et al. 2008).

The motivation in choosing these well-known objects is to refine the previous extinction determinations, by adopting same criteria for selection and analysis of data sets, in order to compare our results with the characteristics of the clusters environments. The paper is organized as follows. Section 2 presents the sample and the information available in the literature for the members of the clusters and the clouds associated to them. Different methods are adopted in Sect. 3, aiming to estimate R_V in the direction of the clusters. Section 4 describes an automatic method to fit the ZAMS reddened colours to the observed data, providing an accurate estimation of visual extinction. In Sect. 5 we develop an analysis of the fractal dimension of the clouds by comparing the spatial distribution of cluster members with statistical parameters related to clustering. The discussion of the results and the conclusions are presented in Sect. 6. The colour diagrams utilized for studying the extinction are presented in the Appendix A.

Table 1. List of the studied clusters.

Cluster	l (°)	b (°)	D (′)	d (pc)	A_V mag	F_{100} 10^7Jy/Sr
Berkeley 86	76.7	+01.3	12	1585[a]	1.7 - 2.5	12-15
NGC 2244	206.3	-02.1	29	1660[b]	0.3 - 2.2	7-20
NGC 2264	202.9	+02.2	39	760[c]	0.9 - 3.8	3-72
NGC 6530	6.1	-01.3	14	1300[d]	3.2 - 4.2	69-500

Columns description: (1) Identification; (2,3) galactic coordinates; (4) diameter; (5) distance obtained from: (a) Bhavya et al. (2007) (b) Johnson (1962), Park & Sung (2002); (c) Sung et al. (1997); (d) Mayne & Taylor (2008).

2. Description of the Sample

The list of clusters and their main characteristics are given in Table 1. This section is dedicated to summarize the information found in the literature, and to describe the adopted criteria in selecting the cluster members and their available observational data. We also performed an analysis of visual extinction maps and far-IR images of clouds against which the clusters are projected.

2.1. Selected Clusters

Berkeley 86 is a particularly small cluster associated to the Cygnus OB1 region. Its youth was revealed by the presence of O type stars, discovered by Sanduleak (1974). Recent results by Bhavya et al. (2007) indicate a distance of 1585±160 pc. They suggest that a low level star formation episode occurred 5 Myr ago, and another more vigorous started during the last 1 Myr. Reipurth & Schneider (2008) presents a comparison of gas and dust distributions in the Cygnus X region, which is influenced by the UV radiation from OB1 association (see their Fig.3). They show that Berkeley 86 is isolated, projected against an area totally free of gas and dust, suggesting low levels of extinction for this cluster. Yadav and Sagar (2001) argue that Berkeley 86 suffers non-uniform reddening with colour-excess varying in the range 0.24 < E(B-V) < 1.01, while Forbes (1981) suggests a more uniform estimation of E(B-V)=0.96±0.07.

NGC 2244 is located at the centre of the Rosette Nebula. It is a prominent OB association probably responsible for the evacuation of the central part of the nebula. The first photometric study of this cluster (Johnson 1962) indicated a colour-excess E(B-V) = 0.46 assuming R_V=3.0 that was later confirmed by Turner (1976) and Ogura & Ishida (1981). Perez et al. (1987) found anomalous R_V for some of the cluster members and suggested the coexistence of main sequence (MS) and pre-MS stars. Román-Zúñiga and Lada (2008) suggest ages of 3±1 Myr. Wang et al. (2008) stud-

ied the X-ray sources detected by *Chandra* in the Rosette region. They verified a double structure in the stellar radial density profile, suggesting that NGC 2244 is not in dynamical equilibrium.

NGC 2264 is one of the richest clusters in terms of mass range, presenting a well defined pre-MS (Dahm 2008). The estimated ages vary from 0.1 to 10 Myr (Flaccomio et al. 1997, Rebull et al. 2002). Surveys in Hα and X-rays revealed the presence of about 1000 members. The cluster is observed projected against a molecular cloud complex of $\sim 2^o \times 2^o$ and is located at 40' north of the Cone Nebula. The interstellar reddening on this cluster is believed to be low: A_V=0.25 estimated by Walker (1954) adopting E(B-V)= 0.082 and R_V=3.08. A more recent work by Rebull et al. (2002) derived A_V=0.45 from a spectral study in a sample with more than 400 stars. Alencar et al. (2010) used the CoRoT satellite to perform synoptical analysis of NGC 2264 with high photometric accuracy. Their results suggest dynamical star-disc interaction for the cluster members, indicating they are young accreting stars.

In the study by Tothill et al. (2008) of the Lagoon Nebula and its surroundings, the main emphasis is given to NGC 6530, a star cluster associated to an HII region that lies at about 1300±100 pc. The estimated age of NGC 6530 is less than 3 Myr (Arias et al. 2007). Despite being in a line-of-sight that contains a high concentration of gas, NGC 6530 appears decoupled from the molecular cloud once the cluster members do not seem to be very embedded. This is consistent with evidences that NGC 6530 is inside the cavity of the HII region (McCall et al. 1990), indicated by measurements of the expanding gas (Welsh 1983). A range of 0.17 to 0.33 mag has been reported for the colour-excess in the direction of NGC 6530 (Mayne & Naylor, 2008). van den Ancker et al. (1997) found a normal extinction law for the intra-cluster region, while Arias et al. (2007) suggest $R_V = 4.6$ for some of the embedded stars. Anomalous extinction has been also reported for cluster members individually, for instance the star HD 164740, for which Fitzpatrick & Massa (2009) suggest E(B-V) = 0.86 and $5.2 < R_V < 6.1$.

2.2. Data extraction and Cluster membership

Two main catalogues of open clusters can be found in the literature: (i) the WEBDA[1] database and (ii) the catalogue DAML02[2] by Dias et al. (2002b) with the compilations: *Tables of membership and mean proper motions for open clusters*, Dias et al. (2002a) based on TYCHO2 and Dias et al. (2006) based on the UCAC2 catalogue.

From DAML02 we searched for clusters with ages up to 10 Myr and distances up to 2 kpc, only selecting those which had members with UBVI photometry and spectral classification available in the WEBDA database. A summary of the characteristics of the sample selected from these two databases is listed in Table 1.

In order to search for relevant information of stars located in the direction of the clusters, three data sets were extracted from WEBDA: (i) UB photometry, (ii) VI photometry, and (iii) equatorial coordinates (J2000). Each source has the same identification in all of these data sets, but the photometry is originated from different works. For the consistency in the data analysis, we selected only cluster memberships having UBVI photometry provided by a single work. The number of studied stars and the corresponding references to the photometric catalogues are listed in Table 2, which also gives information on the number of stars having available spectral data.

[1] www.univie.ac.at/webda/navigation.html
[2] www.astro.iag.usp.br/∼wilton

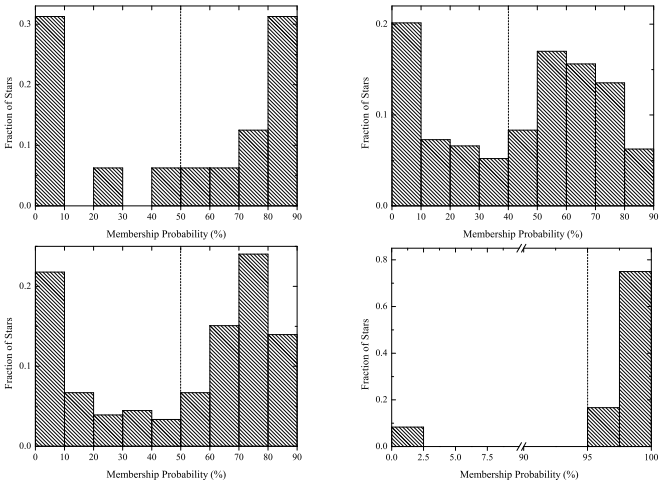

Fig. 1. Normalized number of stars distributed according to membership probability (P%), which is based on their proper motion. A dotted line indicates the minimum probability (P_{min}) that was adopted to separate the most probable members from field stars. Top: Berkeley 86 (left) and NGC 2244 (right). Bottom: NGC 2264 (left) e NGC 6530 (right).

According to Yadav & Sagar (2001) the correct identification of cluster members is crucial for the assessment of extinction in that direction and the most reliable selection is based on kinematic studies (proper motion and radial velocity). DAML02 provides a list of stars with JHK photometry - 2MASS catalogue (Cutri et al. 2003) - and also the probability of the star belonging to the cluster (P%), which is determined from its proper motion. In order to verify if P% is available for our WEBDA sample, their coordinates were compared with those listed by DAML02. A coincidence of sources was only accepted for objects having less than 5 arcsec of difference between coordinates.

The distribution of the number of stars as a function of P% was evaluated on basis of histograms that are presented in Fig. 1. A bimodal distribution is verified, enabling us to distinguish between members and possible field stars. As proposed by Yadav & Sagar (2001), the pollution by field stars should be reduced if only stars with high values of P% are considered members of the cluster. Based on Fig. 1, for each cluster a minimum probability (P_{min}) was adopted to separate field stars, as indicated by dotted lines in the histograms.

The spatial distribution of the stars was also checked looking for possible preferential concentrations, as a function of P%. However, no trend was found in the members distribution.

2.3. Comparison with Molecular Clouds

Extinction caused by interstellar dust found in the line-of-sight can be determined by models that reproduce the

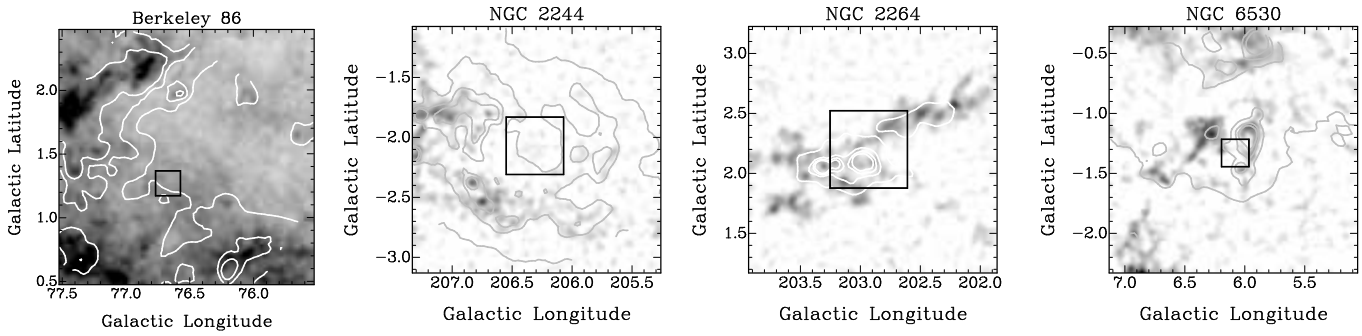

Fig. 2. Map of visual extinction over-imposed by contours measured from IRIS-IRAS images at 100μm band. The contours vary from 50 - 350 MJy/Sr with steps of 100 MJy/Sr, excepting for NGC 6530 that has contours starting at 500MJy/Sr with steps of 1000 MJy/Sr. The area of the cluster is indicated by the black central square.

stars counts in the Galaxy (e.g. Amôres & Lépine, 2005) or maps of visual extinction (Gregorio-Hetem et al. 1988; Schlegel et al. 1998; Dobashi et al. 2005, among others). More recently, colour-excess maps obtained from near-IR surveys have been used to derive the visual extinction in the direction of molecular clouds, as for instance the Trifid nebula, studied by Cambrèsy et al. (2011) based on *2MASS, UKIDSS*, and *Spitzer* data.

Figure 2 displays the position of each cluster projected against the visual extinction map obtained from the 2MASS data (K band). The Catalogue of Dark Clouds by Dobashi et al. (2005) was used to extract the maps for the regions containing our clusters. In order to compare the extinction with the far-IR flux density of the clouds, the A_V maps are over-imposed by contours of IRAS-IRIS data at 100μm. A significant variation of both, A_V and far-IR emission, can be found in the direction of the clusters, excepting Berkeley 86 that appears projected against a uniform field. High levels of far-IR emission are found in the direction of the clusters NGC 6530 and NGC 2264, which coincide with dense regions in the A_V maps. Table 1 gives the ranges of flux at 100μm and A_V in the direction of the clusters. In spite of the sub-structures of the clouds being more evident in K band, we adopted the optical (DSS) maps from Dobashi et al. (2005) to measure A_V.

3. Study of the Extinction Law

3.1. R_V estimation based on colour-excess

One of the methods to obtain R_V uses colour-excess, which can be determined for each cluster member that has well-known spectral type. Intrinsic colours were adopted from Bessel et al. (1998), based on surface gravity and effective temperature that were respectively extracted from Straizys & Kuriliene (1981) and de Jager & Nieuwenhuijzen (1987) as a function of the spectral type and luminosity class available for some stars of the sample.

The expression $\frac{A_\lambda}{A_V} = a(x) + \frac{b(x)}{R_V}$ was adopted from Cardelli et al. (1989) in order to obtain relations between R_V and colour-excess. The results are similar to those based on van de Hulst's theoretical extinction (e.g. Johnson 1968). According to Fitzpatrick & Massa (2009), these theoretical curves seem to be valid only for low- to moderate values of R_V, which tend to be underestimated in the case of anomalous high extinction laws. They suggested a new formula $R_V[K] = 1.36\frac{E(V-K)}{E(B-V)} - 0.79$, which better reproduces the extinction law in different lines of sight.

Due to the lack of spectral type information for our entire sample, we did not determine R_V for each cluster member. Instead of that, we examine the expected ranges of R_V as a function of the distribution of colour-excesses compared to the theoretical extinction laws on the E(V-K) $\times$ E(B-V) plot presented in Fig. 3. An illustration of the dispersion found for R_V[K]=6 is shown by the hatched area, corresponding to the extinction laws given by Cardelli et al. (1989) (upper line) and by Fitzpatrick & Massa (2009) (lower line). For R_V[K]<4 the theoretical lines from both works are quite similar.

Considering the few objects having known spectral type, this analysis cannot be conclusive for our sample, but gives some indication on the variation of E(B-V) and R_V for each cluster. NGC 2264 shows the largest variation, with E(B-V) ranging from 0.01 to 0.3 mag as measured for a sub-sample of 20 stars. A degenerate distribution of R_V is found in this case, spreading from 2.1 to > 6. It can be seen in Fig. 3 that NGC 2264 seems to present a bimodal distribution, where part of the members follows the normal extinction law, while another part has $R_V > 6$.

There are several possible causes to the large variations found in NGC 2264: (i) observational problems that would give inaccurate optical photometry or spectral type determination; (ii) actual variations in each line-of-sight around the cluster area; (iii) anomalies caused by circumstellar environment. In principle, the two first options may be disregarded, since the observational information has been checked in other data sets. Furthermore, there are no correlation between the position of a given cluster member and its R_V. We conclude that a presence of circumstellar matter seems to better explain the anomalies. It can also be noted in Fig. 3 that E(V-K) is particularly large for seven objects of NGC 2264, inconsistent with the low E(B-V) values, suggesting K band excess that is expected in the presence of circumstellar matter. Six of these stars have spectral type later than A0, for which it is important to take into account the errors of spectroscopic data that may cause significant uncertainties on colour excess (see Sect. 3.3). However, it is interesting to note that some of these objects also show an offset from the normal distribution of the observed colours

on TCDs (see Sect. 3.2 and Fig. A2), which is more consistent with individual anomalies of R_V than possible errors on photometry.

Smaller variations are found for the other clusters: members of NGC 2244 have R_V[K] $\sim$ 3.1; NGC 6530 shows a trend to slightly larger values (3.1< R_V[K]<4), while Berkeley 86 tends to have lower values (2.7<R_V[K]<3). However, these results are based on few stars and need to be confirmed by different methods of R_V estimation.

3.2. Two-Colour Diagrams

In order to search for anomalies in the extinction law, we also constructed TCDs following the method proposed by Chini et al. (1983, 1990) and more recently used by Pandey et al. (2000), Jose et al. (2008), Chauhan et al. (2011) and Eswaraiah et al. (2011), among others. TCDs can be used to perform a qualitative analysis of the nature of the extinction by using the relation: $R_c = R_n \times (a_c/a_n)$, where and R_n is the usual normal extinction law, a_c is the slope of the linear fit for the cluster members, and a_n is the slope for field stars.

TCDs use V-λ colours, where λ represents the IJHK bands. In these diagrams the intrinsic colours show a linear distribution up to B-V $\sim$ 1. This limit defines a restricted spectral range of validity, where the ZAMS distribution corresponds to a straight line. In the TCDs, the distribution of field stars is well reproduced by the ZAMS intrinsic colours, once they are reddened by using the mean E(B-V) estimated in the direction of the cluster. In this case, the ZAMS fitting is obtained with R_V=3.1, which we adopted to simulate the distribution of the field stars that must be compared to the cluster members.

The fitting of our sample is restricted to the cluster members having P% > P_{min}, aiming to avoid confusion with field stars. Since the TCD analysis is only valid for a very narrow range of B-V, our calculations are based on objects with spectral type earlier than B8. For each studied band, the slope of the linear fit for the selected cluster members (a_c) was compared to the slope of the normal ZAMS distribution (a_n).

Figures A1 and A2 show the diagrams V-I, V-J, V-H, V-K × B-V, for which a_n is 1.09±0.02, 1.87±0.03, 2.42±0.03 and 2.51±0.04, respectively. The effect of reddening combined with anomalous extinction is illustrated in the V-K × B-V diagrams, where extinction vectors were plotted to represent A_V = 2 mag for two choices of R_V, as used by Da Rio et al. (2010), for instance.

Table 2 presents the results from the TCD analysis giving the fitted line slope in each band, which is used to estimate the mean R_V obtained for the early type stars. Within the estimated errors, a good agreement is found in all bands, excepting NGC 6530. In this case R_V ranges from 4.5 to 6.2. This is the only cluster of the sample clearly showing anomalous extinction law with significant dependence on wavelength. Berkeley 86 and NGC 2264 seems to show a normal law. As verified in Sect. 3.1 (Fig. 3), NGC 2244 also has a bimodal distribution in the TCDs: part of the objects follows the normal law, while other part shows anomalous extinction.

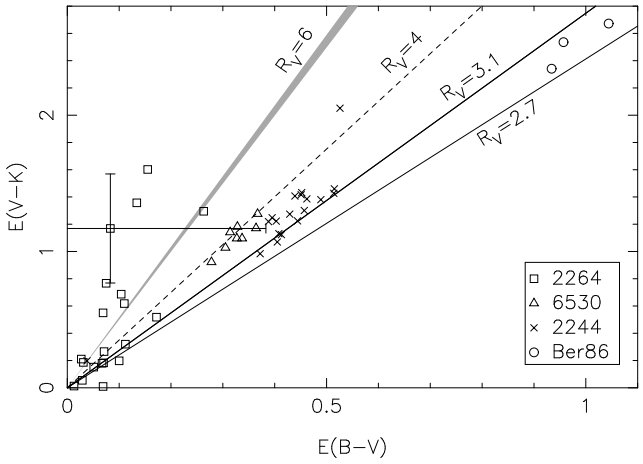

Fig. 3. Different extinction laws compared to the colour-excess distribution for cluster members that have available spectral type. Error bars illustrate the maximum uncertainty expected, if the spectral type is not well determined, for a G8 star.

3.3. Errors estimation

Since our work is based on photometric and spectroscopic data from literature, we have evaluated the global uncertainties taking into account the different sources of errors.

According to the references that provided the photometric data (see Table 2), the error on the magnitudes and colours is ∼0.08 mag in the worst case. Since this value is smaller than the symbol size on the colour-colour diagrams (see Figs. A1 and A2), it does not not affect the linear fitting used to estimate the variations on the extinction law.

Most objects with known spectral types in our sample are O or B type stars, whose errors in the characterization of spectral types are not significant in our calculation of colour-excess. The only exception is NGC 2264 that has some A, F or G stars for which we adopted a maximum uncertainty of two spectral subtypes.

By combining both, spectroscopic and photometric errors, in order to derive colour-excess, we estimate the maximum deviation (the worst case) of 0.3 mag on E(B-V) and 0.4 mag on E(V-K) for a G8 type star of NGC 2264. Considering that we do not use the colour-excess to derive the extinction law, only performing a qualitative evaluation of the expected range of R_V, these errors do not affect the discussion based on colour-excess.

4. Main Sequence Fitting Algorithm

The fit of photometric data to the theoretical isochrones is commonly used to determine star clusters parameters. In order to avoid subjective results that could be derived from visual inspection, different methods of automatic fitting have been proposed to optimize the solution for multivariable fittings. Monteiro et al. (2010), for instance, developed a technique based on the cross-entropy global optimization algorithm. This method proved to be a powerful tool to fit the observed data in colour-magnitude diagrams. More recently, Monteiro & Dias (2011) used this technique to determine open-cluster parameters by using BVRI photometry, which provides reliable estimation of distance, extinction, mass and age.

Table 2. Extinction laws from literature and results obtained from the TCD analysis.

Cluster	N_{tot}	N_{ST}	R_V	a_c[I]	R_V[I]	a_c[J]	R_V[J]	a_c[H]	R_V[H]	a_c[K]	R_V[K]
Berkeley 86	16^a	3^e	3.0^i	1.20	3.39 ± 0.11	1.98	3.29 ± 0.11	2.24	2.87 ± 0.10	2.41	2.98 ± 0.10
NGC 2244	288^b	19^f	3.2 - 3.4^j	1.14	3.22 ± 0.11	2.02	3.36 ± 0.13	2.49	3.19 ± 0.10	2.54	3.13 ± 0.22
NGC 2264	179^c	24^g	3.1 - 5.2^k	1.04	2.94 ± 0.20	1.91	3.17 ± 0.08	2.39	3.07 ± 0.08	2.50	3.09 ± 0.11
NGC 6530	24^d	8^h	3.1 - 5.4^l	1.59	4.49 ± 0.14	3.45	5.73 ± 0.38	4.31	5.52 ± 0.19	5.01	6.19 ± 0.32

Notes: N_{tot} is the total number of studied stars and N_{ST} refers to those having available spectral type, the respective references to photometric and spectroscopic catalogues are: (a) Deeg & Ninkov (1996); (b) Park & Sung (2002); (c) Sung et al. (1997); (d) Sung et al. (2000); (e) Forbes et al. (1992); (f) Johnson (1962), Morgan et al. (1965), Conti & Leep (1974), Hoag & Smith (1959), Wolf et al. (2007); (g) Morgan et al. (1965), Walker (1956), Young (1978); (h) Hiltner (1965). The extinction law references are: (i) Bhavya et al. (2007); (j) Ogura & Ishida (1981), Pérez et al. (1987); (k) Walker (1956), Pérez et al. (1987); (l) Neckel & Chini (1981), Arias et al. (2006).

Since we are interested in solving a single variable problem, we decided to adopt a simple method of fitting. In order to improve the efficiency in determining the visual extinction for the clusters, we developed an algorithm that automatically fits the theoretical ZAMS curve to the observational data in a colour-colour diagram. The best fitting provides the average A_V in the direction of the clusters.

We define $Z_0[ub_i, bv_i]$ as the curve formed by the unreddened ZAMS (Siess et al. 2000) on the U-B × B-V plan (CC diagram). The ZAMS is defined by i=1..n points (intrinsic colours), while the distribution of observed colours is expressed by σ, where $\sigma_j[x_j, y_j]$ is the position occupied by the star j on the CC diagram, with j=1..m. In this case, m is the total number of cluster members.

In order to obtain a reddened ZAMS curve $Z_{A_V}[ub, bv]$ by adding the extinction A_V to $Z_0[ub_i, bv_i]$. The extinction was calculated by using the relation $\frac{A_\lambda}{A_V}$ adopted from Cardelli et al. (1989) and the R_V determined from the TCD analysis (see Sect. 3). The reddened ZAMS was obtained by using $R_V = 3.1$ for NGC 2264, NGC 2244 and Berkeley 86. In the case of NGC 6530 we adopted $R_V = 4.5$ that was estimated from the V-I × B-V diagram.

Following the method proposed by Press et al. (1995), a Cubic Spline interpolation is applied to the reddened ZAMS in order to provide a theoretical curve to be fitted to the observational data. The best fitting is achieved by searching for an A_V that minimizes the distance modulus between the data and the interpolated ZAMS curve, given by:

$$\psi(Z_{A_V}, \sigma) = \sum_{j=1}^{m} (\bar{ub}_j - x_j)^2 + (\bar{bv}_j - y_j)^2$$

where $[\bar{ub}_j, \bar{bv}_j]$ represents the Z_{A_V} point that is closer to $[x_j, y_j]$.

Figure A3 presents the fitting of the observed colours compared to the curve of intrinsic colours on the U-B × B-V diagram. It must be kept in mind that A_V obtained from the ZAMS fitting is only an average. A clear dispersion around this average can be noted in Fig. A3 for NGC 2264 and NGC 2244. According to Burki (1975), a maximum dispersion of ΔE(B-V) = 0.11 may be due to other effects like duplicity, rotation and age differences. This expected dispersion is illustrated by two curves displayed in the bottom panels of Fig. A3. In this case, only cluster members with P%>P_{min} are plotted.

Clusters with uniform or non-variable reddening present a distribution of observed colours falling into the expected range of dispersion. The same cannot be said for several members of NGC 2264 and NGC 2244 that have colours out of ΔE(B-V) = 0.11, which suggest non-uniform reddening.

In summary, the results from the study of extinction law and the main sequence fitting indicate that Berkeley 86 seems to suffer uniform reddening and normal extinction law. NGC 2264 and NGC 2244 also present normal extinction in average, however the reddening is variable for several members of both clusters. NGC 6530 shows anomalous extinction (high R_V) and uniform reddening, as indicated by the small variation of E(B-V).

Our results on reddening are in good agreement with those from literature, as can be seen in Table 3 that gives the colour excesses estimated by: (i) determining the mean value of E(B-V) on basis of spectral type, as described in Sect. 3.1, and (ii) the ZAMS fitting.

In order to verify if the colour-excess measured for the stars is compatible with the extinction effects due to the cloud present in the same line-of-sight, we also present in Table 3 an estimation of E(B-V) that was converted from the extinction map by adopting $R_V = 3.1$ and assuming the minimum and the maximum A_V values given in Table 1.

Since all objects of our sample are very young, they still are physically associated to the cloud complexes where they have been formed, but none of them appears to be deeply embedded. The low extinction of the clouds ($A_V <$ 2.5 mag) in the direction of Berkeley 86 and NGC 2264 (see Table 1) gives E(B-V) similar to the results found in the literature (respectively Forbes 1981 and Johnson 1962), as well as those obtained by us, confirming that they are not surrounded by dense material. When comparing NGC 2264 and NGC 6530 with their respective clouds, it can be noted that both are projected against regions showing high levels of dust emission. The flux at 100 μm reaches 720 MJy/Sr in the case of NGC 2264 and 5000 MJy/Sr for NGC 6530, corresponding to high extinction (A_V = 3.8 and 4.2 mag, respectively) that suggest the presence of large amounts of cloud material. However, both clusters are foreground to these regions, as indicated by the low level of interstellar reddening previously estimated for NGC 2264 (Walker 1956, Pérez et al. 1997, Sung et al. 1997, Rebull et al. 2002) and NGC 6530 (Mayne & Taylor 2008) and confirmed in the present work.

Complementing the study of interstellar reddening, we also performed a fractal analysis that compares the parameters of the clouds with the spatial distribution of cluster members, which has been suggested to be a quantitative method to discuss the relation of environmental conditions with the origin of star clusters, as described in the next section.

Table 3. Colour-excess E(B-V) estimated for the clusters.

	Berkeley 86	NGC 2244	NGC 2264	NGC 6530
Literature	0.96±0.07[a]	0.46[b]	0.06 - 0.15[c]	0.17 - 0.33[d]
S.T.	0.98±0.04	0.42±0.06	0.13±0.03	0.33±0.02
ZAMS	0.89±0.06	0.44±0.06	0.05±0.06	0.21±0.06
A_V Map	0.55 - 0.81	0.12 - 0.71	0.28 - 1.22	1.03 - 1.35

Description of Column 1: *Literature*: E(B-V) given by (a) Forbes (1981), (b) Johnson (1962), (c) Pérez et al. (1987) and Rebull et al. (2002), (d) Mayne & Taylor (2008); *S.T.*: mean results based on spectral type (see Sect. 3.1); *ZAMS*: main sequence fitting (see Sect. 4); A_V *Map*: visual extinction, from Dobashi et al. (2005) map, converted into E(B-V) by adopting normal R_V.

5. Fractal statistic

Aiming to investigate a possible correlation between the projected spatial density of the cluster and its corresponding cloud, we performed a fractal analysis based on the techniques presented by Hetem & Lépine (1993). Our results were compared to artificial clouds and clusters simulated by Lomax et al. (2011) (hereafter LWC11). Both works discuss the behaviour and evolution of molecular clouds under the interpretation of fractal statistic. The fractal dimension measured on realistic simulations of density structures is expected to be related to physical parameters, which are density dependent like cooling function, dissipation of turbulent energy and Jeans limit. However, despite the statistical similarity between fractal and actual clouds, the link between geometry and physics still relies on empirical concepts.

5.1. The perimeter-area relation of the clouds

The clouds studied by LWC11 are artificial, with density profile given by:

$$\rho(r) = \rho_0 \left(\frac{r}{r_0}\right)^{-\alpha}$$

where ρ_0 is the density at $r = r_0$, and α defines the density law. A possible interpretation of α is related to the definition of fractal dimension given by Mandelbrot (1983): $N_M(r) = [\frac{r_0}{r}]^{D_M}$, where $N_M(r)$ represents the number of self-similar structures observed at scale $r < r_0$.

LWC11 adopted a definition of fractal dimension similar to the capacity dimension given by $D = \frac{logN(r)}{log1/r}$, where $N(r)$ is the number of regions of effective side r occupied by data points. A set of points has fractal characteristic if the relation $logN(r) \times log(1/r)$ tends to be linear in a given range of r. The capacity dimension is determined by the slope of this linear distribution (Turcotte 1997).

Our statistical analysis of the clouds is based on the visual extinction maps shown in Fig. 2. The fractal dimension (D_2) of contour levels is measured by using the perimeter-area method described by Hetem & Lépine (1993): $p \propto a^{D_2/2}$, where p is the perimeter of a given A_V contour level and a is the area inside it.

The perimeter-area dimension depends on the resolution of the maps and their signal to noise relation, (Sánchez et al. 2005). We studied $2^o \times 2^o$ regions covered by 123×123 pixels, which gives to all the maps the same resolution ($\sim 0.02^o$ per pixel). Since NGC 2264 is less distant than the other clusters, by a factor of about 2, we have degraded the adopted A_V map in order to simulate a distance of d$\sim$ 1500 pc, which gives a small difference in the measured fractal dimension (within the error bar). In order to minimize errors due to low signal-to-noise ratio (S/N), the lower contour level adopted in the calculation of D_2 was chosen to provide S/N > 10. By this way, the low density regions of the maps were avoided in the calculations.

5.2. The $\mathcal{Q}$ parameter of the clusters

Since stars are formed from dense cores inside molecular clouds, the spatial distribution of young cluster members is expected to be correlated to the distribution of clumps.This correlation can be inferred from the fractal dimension measured on the cloud compared to the $\mathcal{Q}$ parameter measured on the cluster. In the technique proposed by Cartwright & Whitworth (2004), $\mathcal{Q}$ is related to the geometric structure of points distribution and statistically quantifies fractal substructures. Studies on the hierarchical structure in young clusters have used the $\mathcal{Q}$ parameter to distinguish fragmented from smooth distributions (e.g. Elmegreen 2010).

Two parameters are involved in the $\mathcal{Q}$ estimation: $\overline{m}$, the mean edge length, which is related to the surface density of the points distribution, and $\overline{s}$ that is the mean separation of the points. Distributions with large-scale radial clustering, which causes more variation on $\overline{s}$ than $\overline{m}$, are expected to have $\mathcal{Q} > 0.8$. On the other hand, $\mathcal{Q} < 0.8$ indicates small-scale fractal sub-clustering, where the variation of $\overline{m}$ is more important than $\overline{s}$.

The dimensionless measure $\mathcal{Q}$ is given by $\mathcal{Q} = \overline{m}/\overline{s}$, with

$$\overline{m} = \frac{1}{(A_N N)^{1/2}} \sum_{i=1}^{N-1} m_i$$

and

$$\overline{s} = \frac{2}{N(N-1)R_N} \sum_{i=1}^{N-1} \sum_{j=1+1}^{N} |\overrightarrow{r}_i \overrightarrow{r}_j|$$

where N is the number of points in the set, m_i is the edge length of the minimum spanning tree, and r_i is the position of point i. The area A_N corresponds to the smallest circle encompassing all points, with radius defined by $R_N = (\frac{A_N}{\pi})^{\frac{1}{2}}$. To construct the minimum spanning tree, we used the algorithm given by Kruskal (1956) and to determine the smallest circle encompassing all points we adopted the method proposed by Megiddo (1983). This technique was adopted by us and employed to the spatial distribution of the cluster members.

The uncertainties in the estimation of $\overline{m}$, $\overline{s}$ and $\mathcal{Q}$ were calculated by using the bootstrapping method presented by Press et al. (1995). This technique uses the actual set of positions of the cluster members - $\mathcal{S}_0$ with N data points - to generate a number M of synthetic data sets - $\mathcal{S}_1$, $\mathcal{S}_2$...$\mathcal{S}_M$ - also having N data points. A fraction $f = 1/e \sim 37\%$ of the original points is replaced by random points within the limits of the original cluster. For each new set, the parameters $\overline{m}$, $\overline{s}$ and $\mathcal{Q}$ were calculated by adopting M=200. From these measurements, we derived 1 σ deviations $\Delta\overline{m}$, $\Delta\overline{s}$ and $\Delta\mathcal{Q}$ that are presented in Table 4.

Table 4. Statistical parameters obtained from fractal analysis

Cluster	$\mathcal{Q}$	$\overline{m}$	$\overline{s}$	D_2
Berkeley 86	0.73±0.12	0.69±0.12	0.93±0.14	1.39 ± 0.04
NGC 2244	0.75±0.02	0.59±0.02	0.78±0.02	1.37 ± 0.05
NGC 2264	0.76±0.02	0.61±0.05	0.81±0.07	1.47 ± 0.04
NGC 6530	0.85±0.11	0.60±0.10	0.70±0.11	1.34 ± 0.03

5.3. Comparing clouds and clusters

Considering that our calculations are made over two dimension maps, while LWC11 used projections of 3D images, the comparison of measurements of fractal dimension can be done by adopting the equivalence $D_2 \sim D$ - 1.

Figure 4 shows the $\mathcal{Q}$ parameter as a function of fractal dimension obtained by LWC11. In order to illustrate the offset of $\mathcal{Q}$ due to differences on resolution (or number of points), the clustering statistics for fractal distributions (D = 2.0 - 3.0) of artificial data is displayed for two data sets: N=1024 points and N=65536 points. For comparison with our results, the hatched area in Fig. 4 represents the error bars corresponding to the lower resolution data set.

Despite the low number of members studied in our clusters, their distribution are consistent with the LWC11 set of N=1024 points, excepting NGC 6530 that tends to be displaced from the cloud-cluster expected correlation.

Cartwright & Whitworth (2004) suggested that clusters showing central concentrated distributions have $\mathcal{Q}$ increasing from 0.8 to 1.5. On the other hand, clusters with fractal sub-structures have $\mathcal{Q}$ decreasing from 0.8 to 0.45 related to fractal dimension decreasing from $D_2 = 2$ to $D_2 = 0.5$ (we are using here the same relation between 2D images and 3D distributions adopted above). In fact, NGC 6530 is the only cluster of our sample showing indication of radial profile distribution of stars ($\mathcal{Q} = 0.86$), which is not compatible with the fractal structure of its projected cloud ($D_2 \sim 1.3$). The other clusters show members distribution with fractal sub-clustering structure, as indicated by their $\mathcal{Q} < 0.8$ that is in agreement with the fractal dimension measured in the respective projected clouds.

Several works have statistically proved the correlation between fractal dimension, estimated from cloud maps, and $\mathcal{Q}$ parameter, measured on cluster stars distributions. Camargo et al. (2011), for instance, summarizes the concepts first discussed by Lada & Lada (2003) suggesting that the structure of embedded clusters is related to the structure of their original molecular cloud. Fractal structures are observed in clouds showing multiple peaks in their density profile (Cartwright & Whitworth 2004, Schmeja et al. 2008, Sánchez et al. 2010, LWC11).

Based on the comparison with artificial data, we suggest for our clusters a correlation between the fractal statistics of the cloud and the cluster members distribution, excepting for NGC 6530. In this case, the measured fractal dimension does not indicate an uniform density distribution in the cloud, which is expected for associated clusters having central concentrated distributions. For this reason, our fractal analysis indicates that NGC 6530 had a different scenario of formation, when compared to the other three clusters. Our argument for discussing the cluster formation comes from the interpretation of the cloud-cluster relation, which is derived from the fractal analysis. The meaning of this relation is the comparison of the physical structure of the cluster with its remnant progenitor cloud. By this way, the cloud-cluster relation may tell us about the original gas distribution of the cloud that formed the cluster. It also may give us information on how that particular cloud probably evolved since forming the cluster.

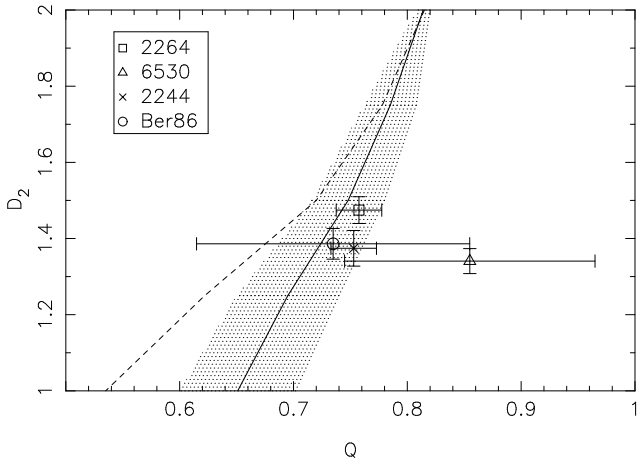

Fig. 4. Comparison of our clusters with the $\mathcal{Q}$ parameter and fractal dimension obtained by LWC11 for artificial data by using different sets of points: N=65536 (dashed line) and N=1024 (full line and respective deviations shown by the hatched area). Symbols with error bars are used to show our results that were estimated from the spatial distribution of cluster members ($\mathcal{Q}$) and projected clouds (D_2).

The concentrated distribution of NGC 6530 indicates an original material more concentrated than the fractal structure of the cloud that remained behind the cluster. Possibly this material was contained in a massive dense core within the cloud, which structure changed due to the process of cluster formation consuming the core. This scenario is consistent with the suggestion that NGC 6530 lies within an HII cavity (McCall et al. 1990).

6. Discussion and Conclusions

We developed a detailed study of the extinction in the direction of four clusters with ages < 5 Myr, located in star-forming regions. The aiming was to search for variable or anomalous extinction that possibly occurs for objects associated to dark clouds. In order to verify the characteristics of the clouds that coincide with the projected position of the cluster, we inspected the visual extinction maps and compared them to the far-IR emission detected in the direction of our sample.

Different methods were used in order to improve previous results on the extinction law R_V, providing means to identify the cause of anomalous extinction. In this comparative study we used the same photometric data base, ensuring similar observational conditions for the entire sample. Theoretical expressions for the extinction law were adopted to evaluate R_V based on the colour-excess E(B-V), which could be determined for some of the cluster members that have spectral type available in the literature. Variable extinction law was clearly verified for NGC 2264, which presented a bimodal distribution. Part of the cluster suffers normal extinction and another part shows large dispersion of R_V values, as illustrated in Fig. 3. However, these results

are not conclusive since few objects had spectral type well determined, particularly Berkeley 86.

A more efficient analysis to estimate R_V and its dependence on wavelength was based on TCDs. The slope of the observed colours distribution, compared to the slope of ZAMS colours in Table 2, indicated anomalous extinction for NGC 6530, which gives $R_V = 4.5$ measured in the I band, and $R_V = 6.2$ in K band. The other clusters have normal extinction, in average. However, some members of NGC 2264 and NGC 2244 appear dispersed in the TCDs, indicating individual anomalous R_V, as illustrated in Figs. A1 and A2. The TCD analysis confirms the results obtained from the colour-excess analysis, based on spectral type. Once there is no relation between the variation of R_V and the spatial distribution of the cluster members, we conclude that differences in the extinction law verified for some cluster members are not caused by environmental differences, but are probably due to circumstellar effects. This is particularly in agreement with the results from Alencar et al. (2010) that confirm the accretion activity in circumstellar discs of NGC 2264 members, for instance.

In order to confirm if our results give reliable reddening correction, the R_V estimated from TCDs was used to determine the visual extinction that best fits the observed colours of the cluster members. A ZAMS fitting algorithm was developed to improve the search for A_V that minimizes the distance of the colours distribution to the reddened ZAMS curve, which was reproduced by Spline interpolation. The best fitting provided a mean value for E(B-V), which was compared to the results from other methods (Table 3). All the colour-excess estimations are in good agreement, excepting the E(B-V) derived from A_V maps mainly for NGC 2264 and NGC 6530. These clusters are not embedded on their respective clouds, which is consistent with the extinction levels found for the cluster members being lower than that measured on the extinction maps for the background stars.

Fractal analysis was performed to investigate the substructures of the clouds and to compare them with statistical parameters of the cluster members distribution. The estimation of the $\mathcal{Q}$ parameter indicated that NGC 6530 has a radially clustered spatial distribution, while the other clusters have fractally sub-clustered distribution of members. The fractal dimension (D_2) measured on the A_V maps, which is related to the cloud geometry, was compared to $\mathcal{Q}$ measured on the clusters distributions. Excepting NGC 6530, the clusters have $\mathcal{Q}$ parameter compatible with the fractal dimension of the corresponding clouds, similar to the distribution of artificial data. We interpreted this result as a correlation between cloud structure and cluster members distribution, which is similar for Berkeley 86, NGC 2244 and NGC 2264. On the other hand, NGC 6530 does not show this cloud-cluster relation, indicating that it was formed from a gas distribution more centrally concentrated, different of the fractal sub-structures found in the remaining cloud.

In fact, even under anomalous $R_V = 4.5$, NGC 6530 does not suffer high extinction, as inferred from the average colour-excess ($A_V \sim 1$ mag), which is incompatible with the high levels of extinction shown in the dark clouds map or the far-IR emission maps. We conclude that anomalous extinction in this case is not due to interstellar dense regions. A tentative explanation is the depletion of small grains due to evaporation that occurs under radiation from hot stars, which is consistent with the location of NGC 6530 in an HII cavity. Neither the circumstellar effects can be disregarded, since the grain growth is expected to occur in protoplanetary discs. In this case, our results are also in agreement with the polarimetric results from McCall et al. (1990) that suggested the anomalous R_V is due to circumstellar effects.

We also verified that the fractal analysis used to investigate the cloud-cluster relation may give some indication about the scenario of the cluster formation. Once the role of this cloud-cluster relation is comparing the physical structure of the cluster with its parental cloud, the interpretation of this relation may tell us about the original gas distribution of the forming cloud and how the particular cloud may have evolved since the cluster was formed. It must be kept in mind that suggesting a cloud-cluster connection based on the correlation of $\mathcal{Q}$ with D_2 is only speculative in the case of our sample, since more points are required to have a robust analysis. However, it is interesting to note the observed trend when comparing calculations performed for data sets from unrelated origins. This trend suggests a connection of stars clustering with sub-structures of the clouds, comparable to the artificial clouds and their derived clusters, studied by LWC11. For this reason, we conclude that NGC 6530 shows actual differences when compared with the other clusters, which is in agreement with previous results from literature.

An interesting perspective of this work is to extend our study to a larger number of clusters, mainly those that have not been studied as well as our sample has been.

Acknowledgements. Part of this work was supported by CAPES/Cofecub Project 712/2011. BF thanks CNPq Project 142849/2010-3. This publication makes use of data products from the Two Micron All Sky Survey, which is a joint project of the University of Massachusetts and the Infrared Processing and Analysis Center/California Institute of Technology, funded by the National Aeronautics and Space Administration and the National Science Foundation.

References

Alencar, S. P. H., Bouvier, J., Catala, C., et al., 2010, in Highlights of Astrophysics, Proceedings of IAU 2009, v. 15, p. 735
Amôres, E. B., & Lépine, J. R. D. 2005, AJ, 130, 659
Arias, J. I., Barbá, R. H., & Morrell, N. I. 2007, MNRAS, 374, 1253
Bhavya, B., Mathew, B., Subramaniam, A., 2007, Bull. Astr. Soc. India, 35, 383
Burki, G. 1975, A&A, 43, 37
Camargo, D., Bonatto, C., Bica, E. 2011, MNRAS 416, 1522
Cambrésy, L., Rho, J., Marshall, D. J., & Reach, W. T. 2011, A&A, 527, A141
Cardelli, J. A., Clayton, G. C., & Mathis, J. S. 1989, ApJ, 345, 245
Cartwright, A., & Whitworth, A. P., 2004, MNRAS, 348, 589
Chauhan, N., Pandey, A. K., Ogura, K., Jose, J., Ojha, D. K., Samal, M. R., Mito, H. 2011, MNRAS 415, 1202
Chini, R., & Krugel, E., 1983, A&A, 117, 289
Chini, R., & Wargau, W. F. 1990, A&A, 227, 213
Conti, P. S., & Leep, E. M. 1974, ApJ, 193, 113
Cutri R.M. 2003, The Two Micron All Sky Survey at IPAC (2MASS), California Institute of Technology
Da Rio, N., Robberto, M., Soderblom, D.R. et al. 2010, ApJ 722, 1092
Dahm, S. E. 2008, Handbook of Star Forming Regions, Volume I, 966
Deeg, H. J., & Ninkov, Z. 1996, A&AS, 119, 221
Dias, W. S., Assafin, M., Flório, V., Alessi, B. S., & Líbero, V. 2006, A&A, 446, 949
Dias, W. S., Lépine, J. R. D., & Alessi, B. S. 2002, A&A, 388, 168
Dias, W. S., Alessi, B. S., Moitinho, A., & Lépine, J. R. D. 2002, A&A, 389, 871
Dobashi, K., Uehara, H., Kandori, R., Sakurai, T., Kaiden, M., Umemoto, T., & Sato, F. 2005, PASJ, 57, 1

Eswaraiah, C., Pandey, A. K., Maheswar, G. et al. 2011, MNRAS (in press)
Elmegreen, B. G., 2010, in Star Clusters: basic galactic building blocks, Proceedings of IAU Symp. No. 266, 2009, R. de Grijs & J. R. D. Lépine, eds., p. 3
Fitzpatrick, E. L., & Massa, D. 2009, ApJ, 699, 1209
Flaccomio, E., Sciortino, S., Micela, G. et al. 1997, Mem. Soc. Astron. Italiana, 68, 1073
Forbes, D., 1981, PASPS, 93, 441
Forbes, D., English, D., De Robertis, M. M., & Dawson, P. C. 1992, AJ, 103, 916
Gregorio-Hetem, J. C., Sanzovo, G. C., & Lépine, J. R. D. 1988, A&AS, 76, 347
Guetter, H. H., & Vrba, F. J. 1989, AJ, 98, 611
Hoag, A. A., & Smith, E. V. P. 1959, PASP, 71, 32
de Jager, C., & Nieuwenhuijzen, H. 1987, A&A, 177, 217
Johnson, H. L. 1962, ApJ, 136, 1135
Johnson, H. L. 1968, in Interstellar Extinction (Nebulae and Interstellar Matter. Library of Congress Catalog Card Number 66-13879), ed. B. M. Middlehurst & L. H. Aller (Chicago, IL: Univ. of Chicago Press), 167
Jose, J., Pandey, A. K., Ojha, D. K. et al. 2008, MNRAS, 384, 1675
Jose, J., Pandey, A. K., Ogura, K. et al. 2011, MNRAS, 411, 2530
Hetem, A. & Lépine, J. R. D., 1993, A&A 270, 451
Hillenbrand, L. A., Massey, P., Strom, S. E., & Merrill, K. M. 1993, AJ, 106, 1906
Kruskal, J. B. J., 1956, Proceedings of the American Mathematical Society, 7, 48
Lada, C. J., & Lada, E. A. 2003, ARA&A 41, 57
Lomax, O., Whitworth, P., Cartwright, A. 2011, MNRAS, 412, 627
Mandelbrot, B.B., 1983, The Fractal Geometry of Nature, ed. W.H. Freeman and Co. (New York)
Mayne, N. J., & Naylor, T. 2008, MNRAS, 386, 261
McCall, M. L., Richer, G. M., Visvanathan, N. 1990, ApJ, 357, 502
Megiddo, N., 1983, Linear-Time Algorithms for Linear Programming in R3 and Related Problems, SIAM Journal on Computing, Vol. 12, 759-776
Melena, N. W., Massey, P., Morrell, N. I., & Zangari, A. M. 2008, AJ, 135, 878
Monteiro, H., Dias, W.S., Caetano, T.C., 2010 A&A, 516, 2
Monteiro, H., & Dias, W.S., 2011 arXiv:1103.3446
Morgan, W. W., Hiltner, W. A., Neff, J. S., Garrison, R., & Osterbrock, D. E. 1965, ApJ, 142, 974
Neckel, T., & Chini, R. 1981, A&AS, 45, 451
Ogura, K., & Ishida, K. 1981, PASJ, 33, 149
Pandey, A. K., Ogura, K., & Sekiguchi, K. 2000, PASJ, 52, 847
Park, B.-G., & Sung, H. 2002, AJ, 123, 892
Pérez, M. R., Thé, P. S., & Westerlund, B. E. 1987, PASP, 99, 1050
Press W., Teukolsky S., Vetterling W., Flannery B., Numerical Recipes in C 2nd edn. Cambridge University Press Cambridge, UK, 1995
Prisinzano, L., Sanz-Forcada, J., Micela, G., Caramazza, M., Guarcello, M. G., Sciortino, S., & Testi, L. 2011, A&A, 527, A77
Rebull, L. M., Makifon, R. B., Strom, S. E. et al. 2002, AJ, 123, 1528
Reipurth, B., & Schneider, N. 2008, Handbook of Star Forming Regions, Volume I, 36
Róman-Zúñiga, C. G., & Lada, E. A. 2008, Handbook of Star Forming Regions, Volume I, 929
Samal, M. R., Pandey, A. K., Ojha, D. K., Ghosh, S. K., Kulkarni, V. K., & Bhatt, B. C. 2007, ApJ, 671, 555
Sánchez, N., Alfaro, E. J., Pérez, E. 2005, ApJ, 625, 849
Sanduleak, N. 1974, PASP, 86, 74
Savage, B. D., & Mathis, J. S. 1979, ARA&A, 17, 73
Schlegel, D. J., Finkbeiner, D. P., & Davis, M. 1998, ApJ, 500, 525
Schmeja, S., Kumar, M.S.N., Ferreira, B. 2008, MNRAS 389, 1209
Setteducati, A.F. & Weaver, H. F. 1962, Berkeley: Radio Astronomy Laboratory, 474, 873
Siess, L., Dufour, E., & Forestini, M. 2000, A&A, 358, 593
Steenman, H., & Thé, P. S. 1991, Ap&SS, 184, 9
Straizys, V., & Kuriliene, G. 1981, Ap&SS, 80, 353
Sung, H., Bessell, M. S., & Lee, S.-W. 1997, AJ, 114, 2644
Sung, H., Chun, M.-Y., & Bessell, M. S. 2000, AJ, 120, 333
Tothill, N. F. H., Gagné, M., Stecklum, B., & Kenworthy, M. A. 2008, Handbook of Star Forming Regions, Volume II, 533
Turcotte, D., 1997, Fractals and Chaos in Geology and Geophysics, Cambridge, Cambridge University Press, pp. 398
Turner, D. G. 1976, ApJ, 210, 65
van den Ancker, M. E., Thé, P. S., Feinstein, A., Vásques, R. A., de Winter, D., Pérez, M. R. 1997, A&AS, 123, 63.
Walker, M. F. 1954, AJ, 59, 333
Walker, M. F. 1956, ApJS, 2, 365
Wang, J., Townsley, L. K., Feigelson, E. D., Broos, P. S., Getman, K., Róman-Zúñiga, C. G., & Lada, E. A. 2008, ApJ, 675, 464
Welsh, B., Y., 1983, MNRAS, 204, 1203
Wolff, S. C., Strom, S. E., Dror, D., & Venn, K. 2007, AJ, 133, 1092
Yadav, R. K. S., & Sagar, R. 2001, MNRAS, 328, 370
Young, A. 1978, PASP, 90, 144

Appendix A: Colour Diagrams

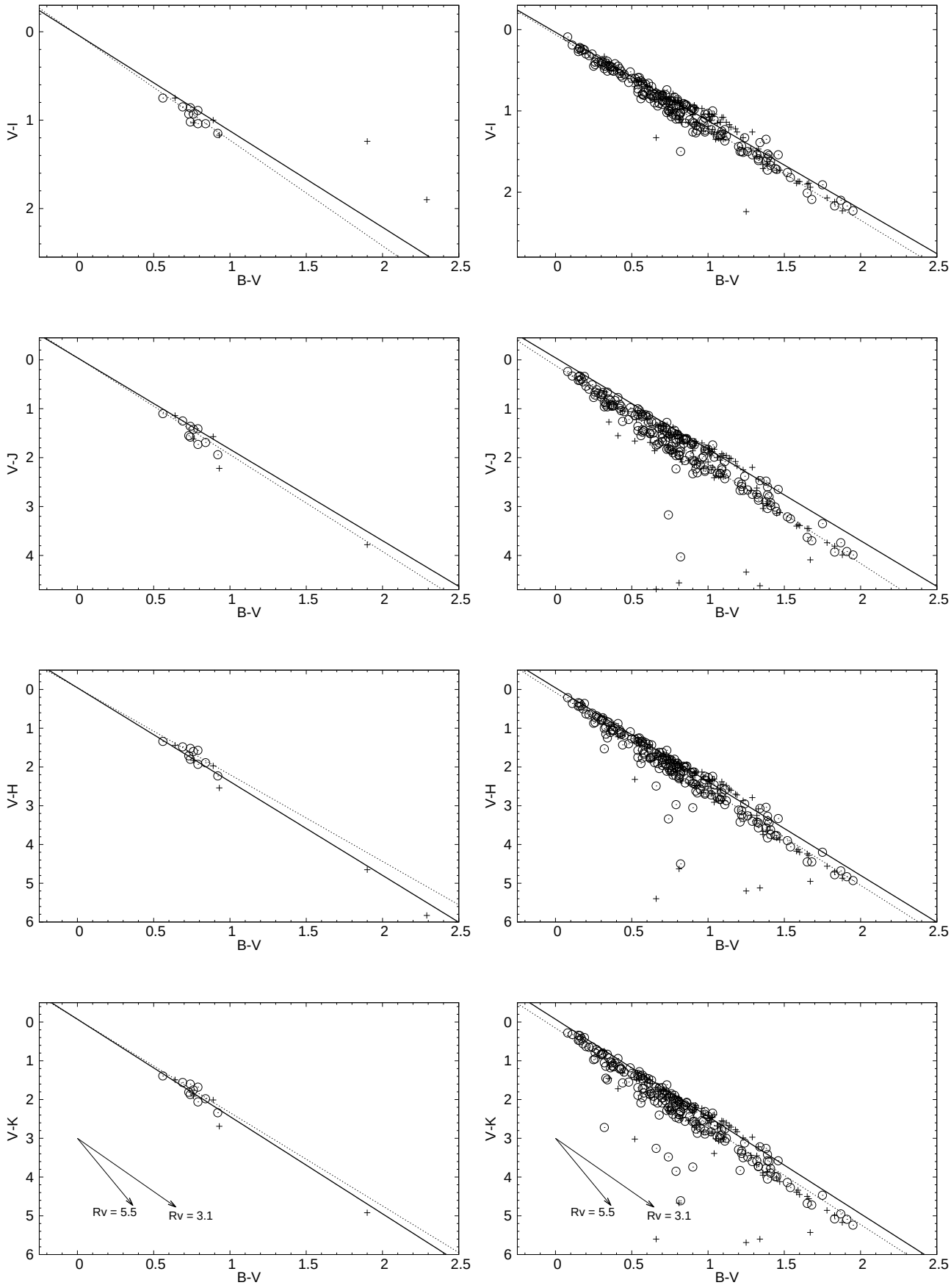

Fig. A.1. TCDs for the clusters Berkeley 86 (left) and NGC 2244 (right). The solid line shows a normal extinction law, while the fitting for the cluster members is shown by a dotted line. Two extinction vectors (A_V = 2 mag) related to different values of R_V are plotted in the bottom panels, for illustration. Open circles indicate the members and crosses show the stars with P%< P_{min}.

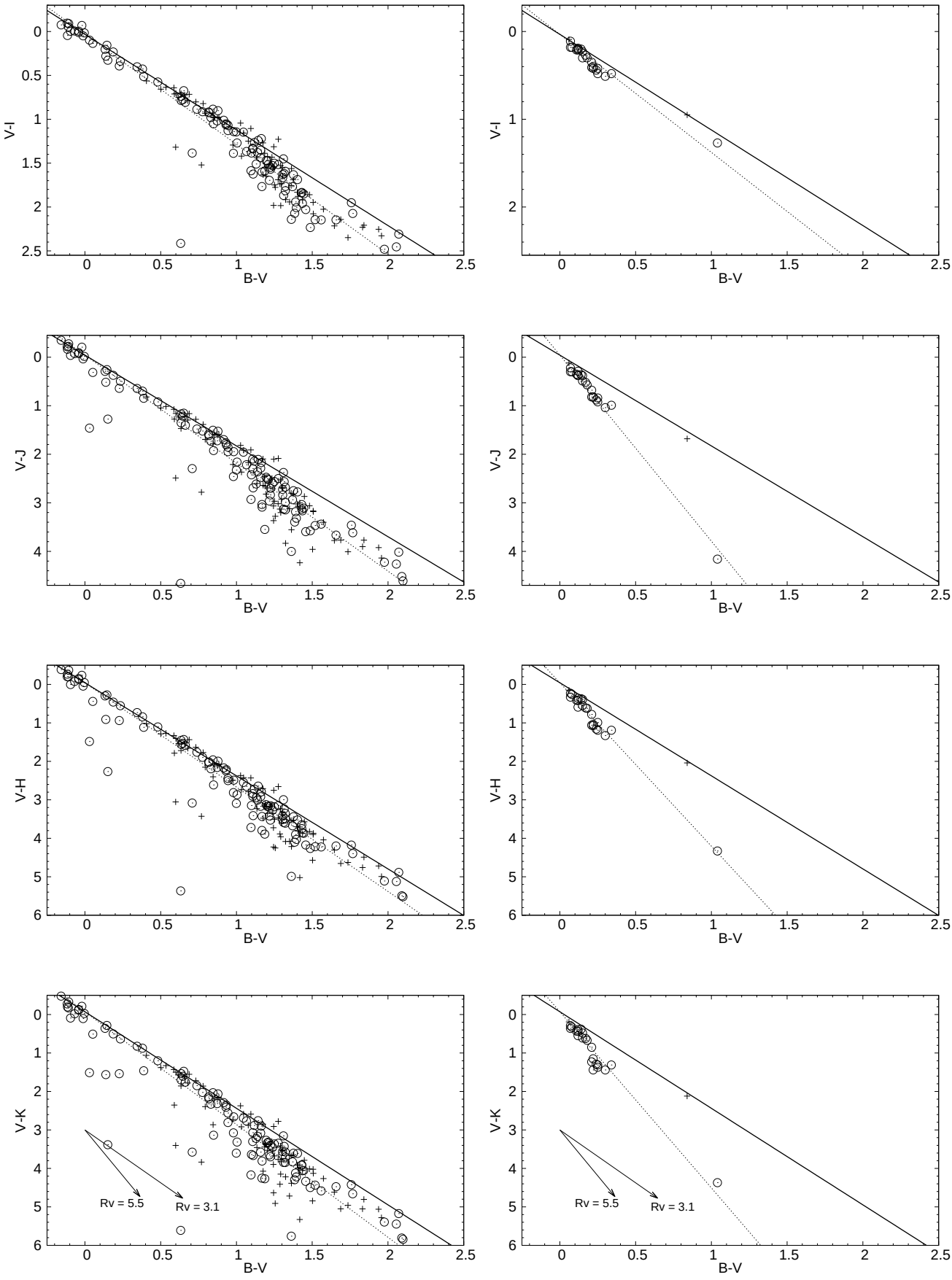

Fig. A.2. TCDs for NGC 2264 (left) and NGC 6530 (right)

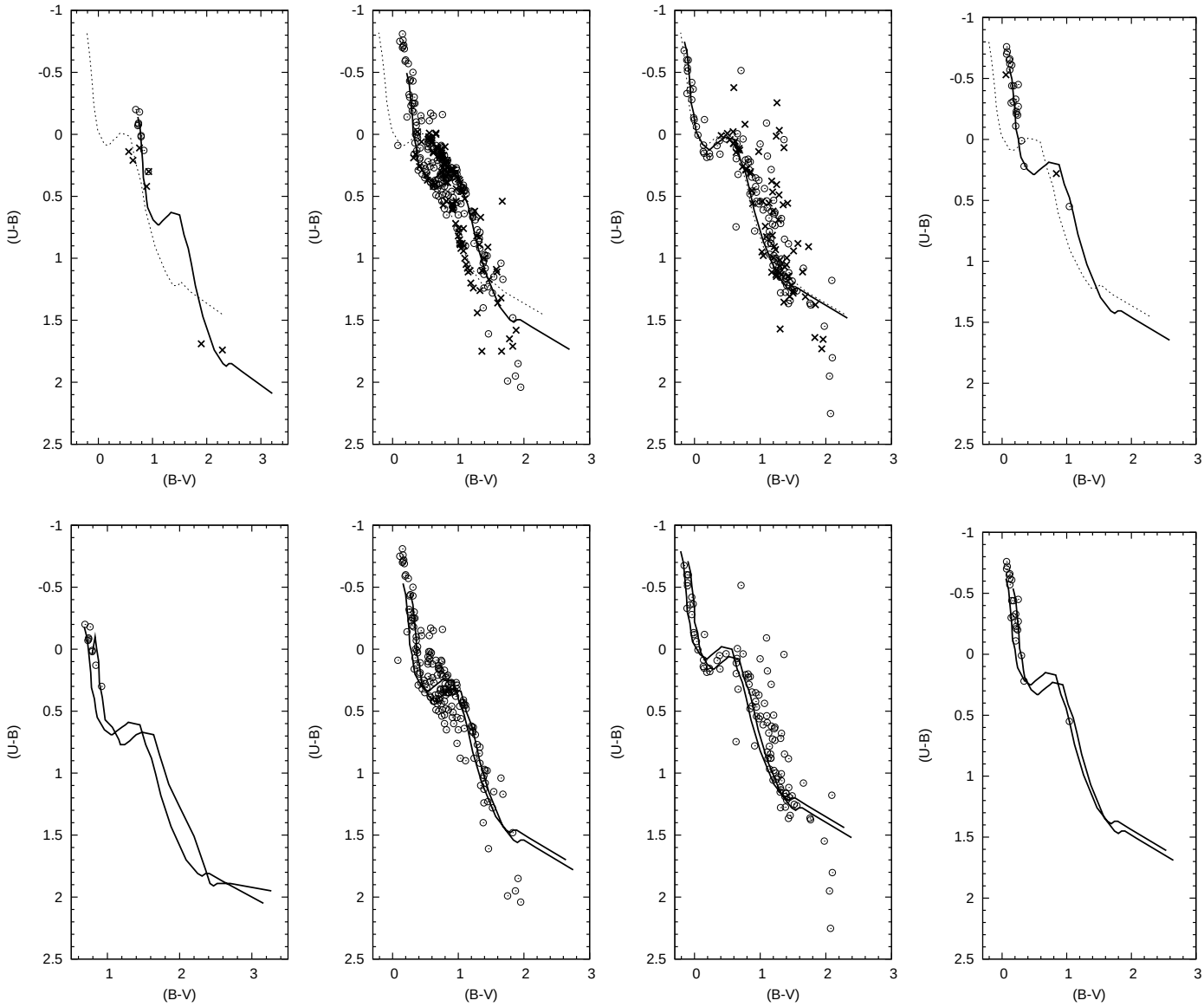

Fig. A.3. Top: Reddened ZAMS fitting to the cluster members with P%>P_{min} (open circles). The position of the other stars of the sample is indicated by crosses. A full line shows the curve obtained with the fitting algorithm, while the dotted line shows the intrinsic U-B and B-V colours. Bottom: Curves representing the limit $\Delta E(B-V) = 0.11$ suggested by Burki (1975). From left to right: Berkeley 86, NGC 2244, NGC 2264, and NGC 6530.